Journal of Magnetic Resonance 301 (2019) 19–29

Contents lists available at ScienceDirect

Journal of Magnetic Resonance

journal homepage: www.elsevier.com/locate/jmr

# DQF *J*-RES NMR: Suppressing the singlet signals for improving the *J*-RES spectra from complex mixtures

Upendra Singh [a,b], Bikash Baishya [a,*]

[a] Center of Biomedical Research (Formerly Centre of Biomedical Magnetic Resonance), SGPGIMS Campus, Raebareli Road, Lucknow 226014, India
[b] Department of Chemistry, Faculty of Science, Banaras Hindu University, Varanasi 221005, India

ARTICLE INFO

*Article history:*
Received 16 October 2018
Revised 21 February 2019
Accepted 22 February 2019
Available online 23 February 2019

*Keywords:*
*J*-RESolved NMR (*J*-RES)
Double-quantum filtered *J*-RES NMR (DQF *J*-RES)
Complex mixture analysis

ABSTRACT

Two-dimensional *J*-RESolved spectroscopy (*J*-RES) finds routine use in metabolomics for reducing signal overlap as it separates chemical shift and multiplet information along two frequency axes. However, only magnitude mode of the experiment is practical which prevents exploitation of its full resolving power. Tailing from high-intensity metabolite peaks often obscure nearby low-intensity metabolite peaks which leads to ambiguity in assignment of metabolites. Absorptive mode *J*-RES spectroscopy offers better-resolving power but comes at the cost of either sensitivity or complicated post-processing. Quite often for certain complex mixtures such as bio-fluids some components of the mixture display intense singlet signals which dominate the whole spectrum resulting in less reliable detection of weaker metabolite signals. Multi-frequency presaturation could suppress these intense singlets but will also remove the useful weaker multiplet peaks which are either totally eclipsed with the intense singlets or very close in frequency. We show that by using a double quantum filter (DQF) in magnitude mode *J*-RES technique, the intensity of the strong singlet metabolite peaks can be reduced relative to the intensity of the sparsely present multiplet metabolite signals. This approach leads to the identification of many weak intensity multiplet peaks which are otherwise undetected due to their overlap with intense singlet peaks in regular *J*-RES as well as 1D $^{1}$H spectra. Although the improved intensity of most of the weaker peaks relative to the strong singlet peaks is observed, some multiplets can disappear due to the delay-dependent modulation of the signals by the DQF. A few DQF *J*-RES spectra recorded with different DQF delays, therefore, produce better assignment when analyzed together. The technique is demonstrated on a mixture of eight compounds, human urine, and plant extract samples.



## 1. Introduction

*J*-RES spectroscopy finds widespread use in chemical, biological, medical, and environmental studies. This method finds routine use in chemistry for measurement of accurate *J*-couplings and also for resolving peaks in crowded spectral regions. Although one-dimensional (1D) $^{1}$H NMR spectroscopy is the most reliable technique in metabolomics due to the rapid acquisition and straightforward quantitative aspects; nevertheless, severe spectral overlap of the peaks is a bottleneck to the identification and quantification of a large number of metabolites. *J*-RES NMR overcomes this spectral congestion greatly by spreading the chemical shift and multiplet information along two orthogonal frequency axes. As a result, *J*-RES NMR spectra have found widespread use in NMR based metabolomics for metabolic profiling studies of biofluids [1–14], like human urine [2] plasma [3,9], cerebrospinal fluids [4]. Diverse studies on plants [10], fish [11], beer [12], tissues [14], kinetic drug metabolism [13], etc. have been carried out by *J*-RES NMR spectroscopy. All such studies have highlighted the advantage of improved peak dispersion in *J*-RES NMR by reducing peak overlaps in highly overlapped regions [1,7]. Improved peak dispersion in projected *J*-RES spectra has been demonstrated to enhance the quality and interpretations of multivariate models such as PCA (Principal Component Analysis) and statistical correlation analyses such as STOCSY (statistical total correlation spectroscopy) [1,7]. *J*-RES spectroscopy has also been used to distinguish enantiomers in chiral aligned media [15–17], to extract one-bond heteronuclear couplings in large macromolecules [18,19], and to improve resolution in DOSY-type experiments [20].

However, the full potential of the *J*-RES technique remains underexploited. The dispersive phase twisted lineshape inherent to the technique renders absorption mode representation of the spectrum ineffective. As a result, only the absolute value of the

* Corresponding author.
*E-mail addresses:* bikashbaishya@gmail.com, baishyab@cbmr.res.in (B. Baishya).

https://doi.org/10.1016/j.jmr.2019.02.003
1090-7807/

complex spectra are in routine use. Since the dispersive Lorentzians are broader compared to absorptive Lorentzians, the absolute value mode 2D *J*-RES spectrum in general display broad peaks sacrificing much of the potential high resolution that could be achieved if the dispersive contribution could be suppressed. The problem gets further aggravated in complex mixtures where the concentration of certain metabolites is much higher than the rest. Thus, the broad dispersive tails from the strong peaks obscure the low-intensity peaks in the neighborhood. This often leads to ambiguity in the assignment of metabolite peaks.

Several attempts have been made over the years for producing absorption mode 2D *J*-RES spectra- modified pulse sequences to suppress the dispersive terms [21–23], combined data manipulation and pattern recognition [22], purely data post-processing [24], adiabatic z-filtered *J*-RES spectroscopy with multiplet reduction algorithm [25], and recent absorptive *J*-RES spectroscopy by using homo-decoupling schemes such as BASHD (Band Selective Homodecoupling) [26], PSYCHE (Pure Shift Yielded by Chirp Excitation) [27], ZS (Zangger and Sterk) [21] and BIRD (Bilinear Rotation Decoupling) [28]. These approaches have not found routine use as either lower sensitivity (10–20% of regular proton sensitivity at best), complicated optimization and post-processing, and longer experimental time hampers their efficiency. In overall, the regular magnitude mode *J*-resolved technique is extensively used in all applications due to higher sensitivity, better resolution compared to 1D $^1$H NMR, and simpler execution features.

In the present work, we overcome one key limitation of regular magnitude mode *J*-RES NMR without attempting absorptive mode representation and without losing much of its sensitivity. In metabolomics as well as other applications that involve complex mixtures, quite often some components of the mixture display very high-intensity singlet peaks owing to their high abundance in the mixture and a single spectral line instead of a multiplet. This is particularly observed for complex mixtures such as human urine (where the creatinine singlet peaks generally dominate the whole $^1$H 1D spectrum) and many other samples. The whole $^1$H 1D spectrum is dominated by the intense singlet peaks resulting in the lower intensity of the weaker signals present in the spectrum, and the same is true of 2D *J*-RES spectrum. Any weak intensity multiplet peak close to the intense singlet signals gets obscured in the 2D *J*-RES spectrum. While presaturation at multifrequency or WET technique [29] can be used to suppress such multiple intense singlets, that way one will also eliminate any important multiplet peaks which are eclipsed by the strong and broad singlet resonances. In the present work, we show that a double-quantum filter (DQF) [30–35] when combined with regular magnitude mode *J*-RES technique can greatly reduce the intensity of the singlet resonances leading to better resolution of any weak multiplet peak which is either eclipsed or adjacent to the intense singlet metabolite peaks. High-quality *J*-RES spectrum from three samples- a mixture of eight compounds, human urine, and a plant extract are reported. It is worthwhile to mention that the double-quantum filter has also been used in COSY-DOSY experiment to increase the validity of monoexponential fits for the determination of diffusion coefficients in complex mixtures [36]. Recently, the intermolecular double-quantum coherence based *J*-RES spectroscopy has also been demonstrated for overcoming line broadening induced by variations in susceptibility in intact biological tissue samples. This method utilizes the fact that intermolecular multiple-quantum coherences arising from distant dipolar interactions in such semi-solid samples do not suffer from the field inhomogeneities [37,38].

## 2. DQF *J*-RES pulse sequence

Fig. 1 displays the pulse sequence for acquiring Double Quantum Filtered (DQF) 2D *J*-RES spectrum. It involves the application of a DQ filter before the evolution period of the *J*-RES sequence to eliminate the intense singlet signals. The narrow rectangular bars are nonselective 90° pulses while broad rectangular bars are refocusing nonselective 180° pulses. CW represents continuous wave for pre-saturation of water signal during recycle delay. The first gradient $G_5$ dephases any components of transverse magnetization which may be present due to the previous scans and allows only longitudinal magnetization (along the z-axis) to take part in the pulse sequence. The first 90° pulse between the time points 'a' and 'b' creates the signals denoted by $I_{1y}$, $I_{2y}$, $I_{3y}$. . .. at time point 'b.' During time period 2Δ from 'b' to 'c' these signals evolve into antiphase coherences such as $I_{1x}I_{2z}$, $I_{2x}I_{1z}$, $I_{3x}I_{4z}$ under homonuclear scalar couplings to adjacent signals. The second 90° pulse between time points 'c' and 'd' creates all kinds of multiple-quantum coherences such as $I_{1x}I_{2y}$, $I_{2x}I_{1y}$, $I_{3x}I_{4y}$. The third 90° pulse between time points 'e' and 'f' flanked by gradients in the ratio of $G_1$:2$G_1$ (coherence selection gradients) are used to select only double-quantum coherences present between time points 'd' and 'e' as in DQF-COSY. This suppresses the strong singlet resonances from the final spectrum. Again during the time period 2Δ from time point 'f' to 'g' (as $\Delta_1$ is a small delay of 1 ms) the signals evolve under scalar coupling and refocus to the initial terms $I_{1y}$, $I_{2y}$, $I_{3y}$. . .. etc. at time point 'g.' Due to the difference in the magnitude of scalar couplings between different signals all antiphase coherences does not get refocused to inphase coherences. Hence, the fourth 90° pulse between time points 'g' and 'h' creates the terms $2I_{1x}I_{2y}$ and $I_{1z}$ (and similar terms for other signals) from the antiphase and desired inphase coherences respectively at time point 'h.' The gradient $G_0$ between time points 'h' and 'i' is used for dephasing all transverse components of magnetization. The final terms left at time point 'i' are Z-spin orders such as $I_{1z}$, $I_{2z}$, $I_{3z,}$ etc. A zero-

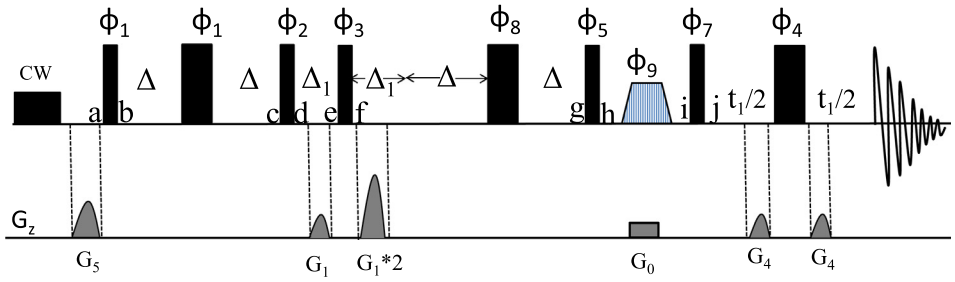


**Fig. 1.** The pulse sequence for DQF *J*-RES spectroscopy. The narrow rectangular bars are nonselective 90° pulses while broad rectangular bars are refocusing nonselective 180° pulses. CW represents continuous wave for pre-saturation of water signal during recycle delay. The delay 2Δ is tuned to 40 ms. $G_5$ (=30.5G/cm) and $G_0$ (=25.1G/cm or 0.8G/cm for ZQ filter) are dephasing gradient. $G_1$ (22.7G/cm) and $G_1$*2 are used to select the DQ coherences. $G_4$ (=8.3G/cm) flanked by the refocusing pulses are coherence selection gradient for the signals that go through an echo. A zero-quantum filter can also be applied between time points 'h' and 'i'. However, this is optional for magnitude mode *J*-RES spectroscopy as any residual signal via ZQ pathway does not interfere with the multiplets generated by $t_1$ modulation of the scalar coupling interaction.

quantum filter can also be applied between time points 'h' and 'i' shown with trapezoid shape to improve the spectrum. However, this is optional as any residual signal via ZQ pathway does not interfere with the multiplets in a magnitude mode *J*-RES spectroscopy. The last 90° pulse is applied between time points 'i' and 'j' which starts the same time events as in regular *J*-resolved sequence. The nonselective refocusing pulse flanked by the $G_4$ gradients at the centre of the $t_1$ dimension ensures the evolution of only homonuclear scalar couplings leading to the final terms as $I_{1y}$ and $-2I_{1x}I_{2z}$ and similarly for other signals such as $I_2$, $I_3$, etc. Low power CW presaturation was also applied during the Δ delays to suppress the water signals.

## 3. Experimental

### 3.1. Sample preparation and data acquisition

All the one and two-dimensional experiments reported in this paper were carried out on an 800 MHz NMR spectrometer equipped with a CPTCI cryoprobe with z-axis gradient only at 300 K temperature. All *J*-resolved spectra were acquired and processed in magnitude mode. Three samples were targeted for evaluating the performance of our new technique- a mixture of eight compounds as detailed below, one human urine sample, and an extract of G. Pedunculata dried fruit which represents complex metabolomics mixture.

### 3.2. A complex mixture of eight metabolites

A complex mixture designated as **1** was prepared by mixing the following compounds- valine, tyrosine, phenylalanine, tryptophan, betaine, creatinine, cysteine, and acetylacetone in 500 μL of $D_2O$ and 500 μL of phosphate buffer (pH = 7.0). The final concentration of the solution was: 8.5 mM of valine, 4.9 mM of tyrosine, 7.8 mM of phenylalanine, 24 mM tryptophan, 83 mM for betaine, 62 mM for creatine, 9 mM for cysteine and 49 mM for acetylacetone. Finally, the 500 μL solution was transferred to a 5 mm NMR tube for NMR experiment. Regular 2D *J*-RES spectrum displayed in Fig. 2a) was recorded on this mixture with the following acquisition and processing parameters: $t_1$ and $t_2$ acquisition times of 392 ms and 369 ms respectively, spectral width 8333 Hz in $F_2$, and 48 Hz in $F_1$ dimension, number of transients was 16. Zero-filled to 16,384 and 128 data points in $F_2$ and $F_1$ dimension respectively. Processed with unshifted sine bell window functions in both $F_2$ and $F_1$ dimensions in magnitude mode. DQF-*J*RES spectrum shown in Fig. 2b was acquired with the same acquisition, and processing parameters as above except the number of transients were 32 per increment. Total experimental time was 29 min 48 s for magnitude mode 2D *J*-RES experiment and 1 hr and 1 min for DQF-*J*-RES experiment. The 2Δ delay was tuned to 40 ms. Gradients used in regular 2D *J*-RES experiment were 15% (=8.3G/cm) before and after the refocusing pulse with shape SINE.100. Gradients used in DQF *J*-RES NMR are $G_1$ = 42.5% (=22.7G/cm), $G_0$ = 47% (=25.1G/cm) or 1.5% (=0.8G/cm for ZQ filter), $G_4$ = 15% (=8.3G/cm) and $G_5$ = 57% (=30.5G/cm).

### 3.3. Dried fruit extract of G. Pedunculata

The dried, ground fruit of *Garcinia Pedunculata* weighing 5 g was subjected to extraction in a Soxhlet apparatus using 50 mL of non-polar solvent n-hexane for 12 h. The solvent was evaporated by rotary evaporator. 500 μL of $CDCl_3$ was added to the dried sample, and this solution was taken into a 5 mm NMR tube for NMR experiment. Regular 2D *J*-RES spectrum of dried fruit extract displayed in Fig. 4(a), (c), (e), and (g) was acquired with $t_1$ and $t_2$ acquisition times of 392 ms and 428 ms respectively, with a spectral width of 8333 Hz in $F_2$-dimension and 70 Hz in $F_1$-dimension, number of transients was 32. The spectrum was zero-filled by 16,384 and 128 data points in $F_2$ and $F_1$ dimensions respectively. The spectrum was processed with unshifted sine bell window functions in both $F_2$ and $F_1$ dimensions in magnitude mode. DQF *J*-RES spectrum displayed in Fig. 4b, d, f, and h was acquired with the same parameters as mentioned above except the number of transients were 64 per increment and 2Δ delay of 40 ms. Total experimental time was 1 h and 31 min for magnitude mode 2D *J*-RES experiment and 3 h and 11 min for Double Quantum Filtered 2D *J*-RES spectrum. Same gradients were used as in the DQF *J*-RES sequence mentioned above.

### 3.4. Lyophilized human urine sample

Human urine from a volunteer was collected and kept at −80 °C deep freezer. Approval was taken for NMR method development on bio-fluids as per Institute Ethics Committee (Letter No. B17/CBMR/IEC/EMP/5/2017). The sample was thawed, and 1 mL of the urine sample was taken for further processing. The sample was centrifuged at 12,000*g* for 5 min, and the supernatant was collected. The supernatant was frozen at −80 °C again and put it into Lyophilizer for getting the powder form. The powder was mixed with 260 μL $D_2O$ and 260 μL Buffer of pH = 7.4. The solution was centrifuged at 12,000*g* for 5 min. 500 μL Solution was taken into 5 mm NMR tube for NMR experiments. Regular 2D *J*-RES spectrum of Lyophilized human urine shown in Fig. 6(a), (c), (e), (g), (i) and (k) was acquired with $t_1$ and $t_2$ acquisition times of 392 ms and 369 ms respectively, with spectral width of 8333 Hz in $F_2$, and 65 Hz in the $F_1$ dimension, the number of transients was 64. Zero-filled to 16,384 and 128 data points in $F_2$ and $F_1$ dimension respectively. Regular 2D *J*-RES spectrum was processed with unshifted sine bell window functions in both $F_2$ and $F_1$ dimensions in magnitude mode. DQF 2D *J*-RES spectral portions displayed in Fig. 6(b), (d), (f), (h), (j) and (l) was acquired with the same acquisiton and processing parameters as mentioned above. Total experimental time was 1 h and 57 min for regular *J*-RES experiment and 2 h and 4 min for DQF *J*-RES. Same gradients were used as in the DQF *J*-RES sequence mentioned above, and 2Δ delay of 40 ms was used.

## 4. Results and discussion

### 4.1. Application to a complex mixture of eight metabolites

The 45° tilted magnitude mode *J*-RES spectra of the mixture **1** are displayed in Fig. 2(a) and (b) from regular *J*-RES sequence and DQF *J*-RES sequence respectively. Small portions of the spectra marked with P, Q, R, and V from (2a) (from regular *J*-RES) are shown expanded in Fig. 2(c) and (e) respectively with dotted boxes. The same portions in (2b) (from DQF *J*-RES) are marked with S, T, U, and W and shown expanded in Fig. 2(d) and (f) respectively. Comparisons of the spectral portion R vs. U (in 2c vs. 2d)), and also V vs W (in 2e vs 2f) reveals the superior quality spectrum from DQF *J*-RES sequence- the tyrosine and valine multiplets along $F_1$ are obscured in the regular *J*-RES spectrum due to overlap with the creatine and acetylacetone strong singlet peaks respectively, but get well resolved in DQF *J*-RES spectrum due to the efficient suppression of the strong singlet peaks. Assignment of the peaks are shown in (2d) and (2f). Inspection of the spectral region inside box U in 2d reveals the significantly enhanced intensity of the tyrosine multiplet relative to the creatine singlet. However, the singlet peak from creatine methyl peak in the box R in (2c) is very high in intensity compared to the overlapped multiplet from tyrosine geminal

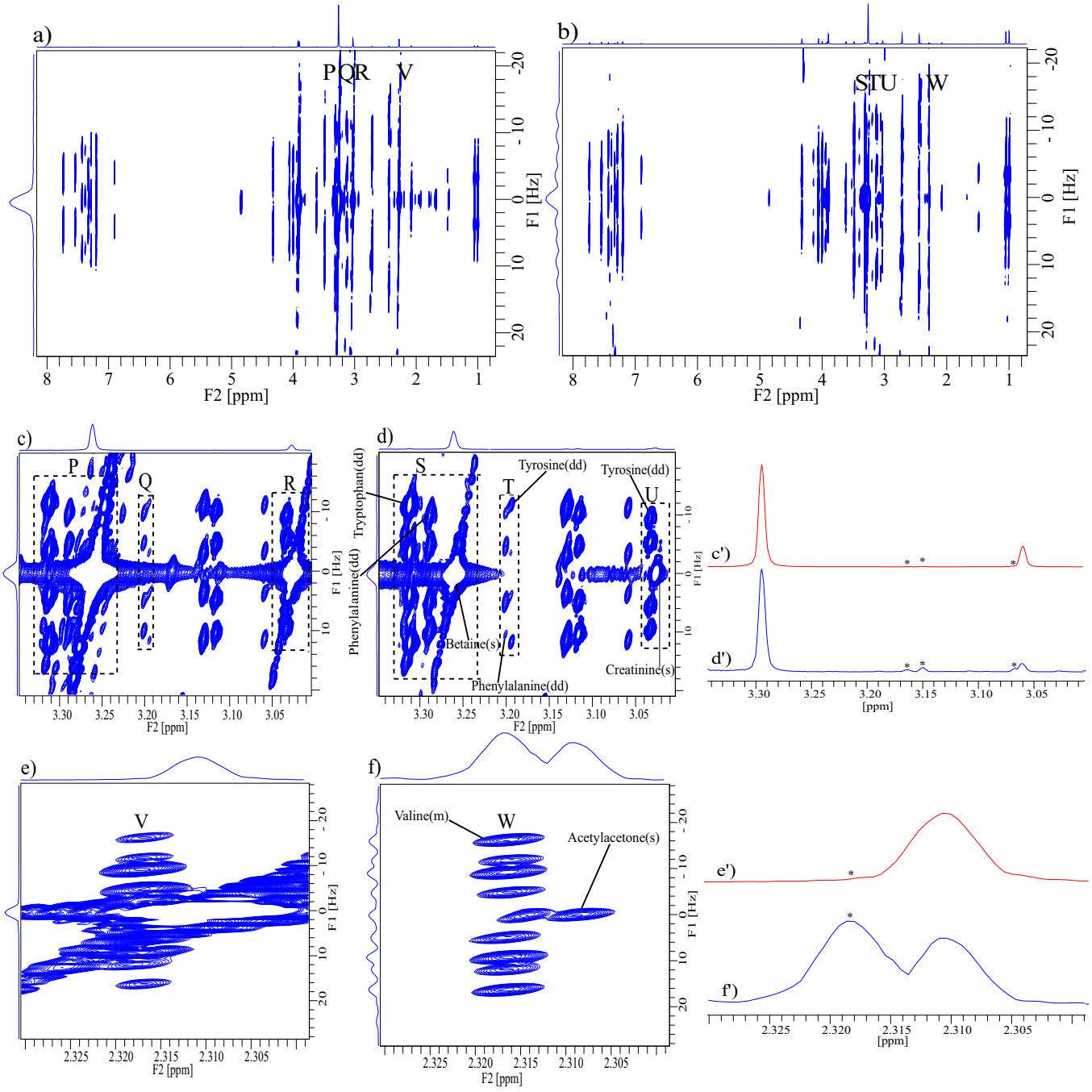


**Fig. 2.** (a) and (b) are the 45° tilted magnitude mode *J*-RES spectrum and DQF *J*-RES spectrum of the mixture **1** respectively. Small portions of the spectra marked with P, Q, R, and V in (a) are shown expanded in Fig. 2(c) and (e) respectively with dotted boxes. The same portions in (b) are marked with S, T, U, and W and shown expanded in Fig. 2(d) and (f) respectively. Panel 2c shows intense singlet peak and its tail along $F_1 = 0$ obscuring the multiplet information inside the dotted boxes P, Q, and R. Panel 2d shows that the intensity of the singlet peaks along $F_1 = 0$ is reduced and the multiplet information such as dd of tyrosine inside dotted box U is revealed clearly. The clarity of the multiplets inside the dotted boxes S and T also improves. Comparison of the 1D projections from the 2D portions (c) and (d) are shown in (c′) and (d′) respectively which reveals improved visibility of the multiplets in DQF projection (shown with a star mark) in d′) relative to the singlets (without star mark). Panel (2e) from regular *J*-RES 2D portion V shows a multiplet overlapped with an intense singlet which does not allow extraction of the *J*-coupling information. Panel (2f) from DQF *J*-RES improves the intensity of the multiplet relative to the singlet and the ddd pattern from valine can be clearly assigned. Comparison of the projections (e′) and (f′) from (e) and (f) also reveals better visibility of the ddd peak (star mark) of valine relative to the singlets. Thus, reduced dynamic range issues in DQF *J*-RES improves assignment.

proton as the concentration of creatine in the mixture were almost 12 times higher than tyrosine. Similarly the acetylacetone singlet peak in the box W (in 2f)) becomes very weak relative to the valine multiplet peak after the application of DQF. In contrast, the same acetylacetone singlet peak in box V in regular *J*-RES spectral portion is quite intense relative to the valine multiplet as the concentration of the former was 6 times higher than the later. Comparison of the spectral region inside dotted box portions P vs. S shows suppression of strong singlet peak in DQF *J*-RES spectrum and hence more clarity of the two doublet of doublets (from Tryptophan and phenylalanine showed in dotted box S) in the neighborhood. A similar comparison of the peaks inside dotted boxes Q and T shows that the two doublet of doublets from tyrosine and phenylalanine are better read out from DQF *J*-RES spectrum. In regular

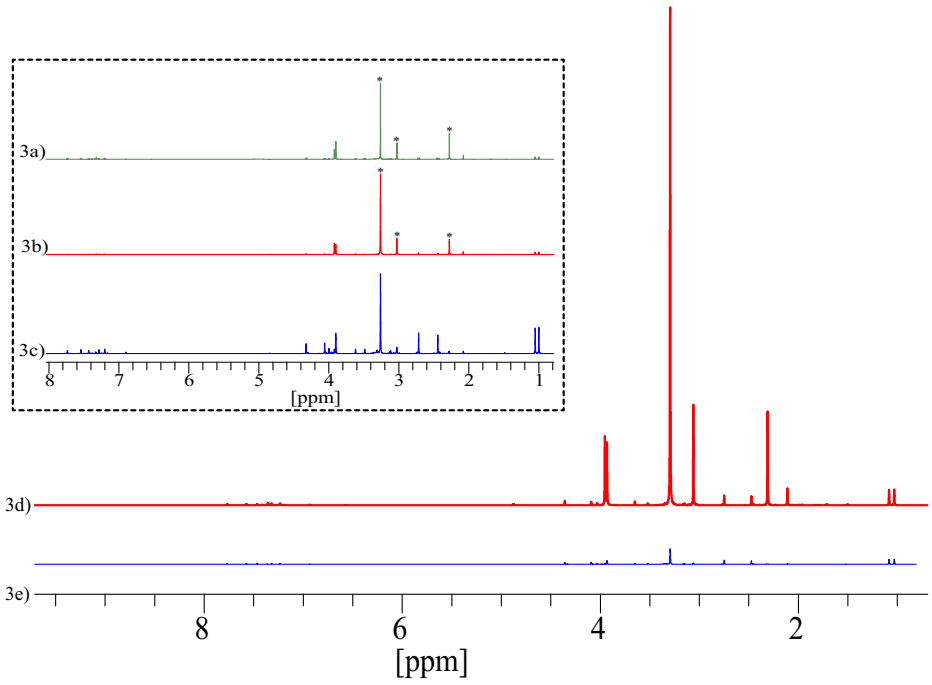


**Fig. 3.** a, b, and c are a comparison of regular $^{1}$H NMR with presaturation, regular *J*-RES projection, and DQF *J*-RES projection respectively from the amino acid mixture compared for the same intensity of the most intense singlet peak. The comparison reveals few intense singlet signals marked with a star (at 3.24, 3.0, 2.26, ppm) dominate the regular $^{1}$H NMR (a) and regular *J*-RES projection (b). In contrast, DQF *J*-RES projection in c shows great improvement in the intensity of the smaller signals relative to the curtailed singlet signals marked with a star. (d) and (e) is a comparison on the same noise level of the regular *J*-RES projection and DQF *J*-RES projection, which shows much higher S:N of the regular *J*-RES projection. Measurement of S:N for four peaks reported in SI Table S1 revealed regular *J*-RES has on average much higher S:N relative to the DQF *J*-RES projection despite the later had two times higher transients. The improved receiver gain 203 in (3e) relative to 20.3 in regular *J*-RES (3d) improves the digitization of the smaller signals compared with the noise. This gain combined with suppression of the intense singlet peaks improves the visibility of the weak intensity metabolite peaks in DQF *J*-RES spectrum. This is also clearer from the analysis of the 2D spectral portions in Fig. 2c–f.

*J*-RES spectrum, the strong tail from the singlet at zero frequency along $F_1$ can lead to ambiguity in assignment when a multiplet component is buried inside it. Suppression of singlet intensity to almost null clears such ambiguity. Comparison of the 1D projections from 2c and 2d are shown in 2c′ and 2d′ respectively for the comparable intensity of the larger signals. Similarly, 2e and 2f are shown in 2e′ and 2f′ respectively. Comparison of these projections reveals improved visibility of the multiplet peaks marked with a star in the DQF projections relative to the singlet peaks (without star) in the regular *J*-RES projections. The receiver gain value got optimized to 20.3 in (a, c, e) in regular *J*-RES, a small value for the observation of the smaller signals. In contrast, the DQF *J*-RES optimized this value to 203 (in b, d, and f) which improved the visibility of the smaller signals. Thus, the singlet peaks combined with the higher concentration of that metabolite leads to severe spectral readout problem for the weaker peaks due to their order of magnitude higher intensity than the weaker multiplets from the less abundant metabolites. The DQF filter scales down all singlet peaks (more than the multiplet peaks) revealing the weaker multiplet structures clearly. Although on the absolute S:N scale (as is shown in next section Fig. 3) the DQF *J*-RES is a poor spectrum, however, suppressing the intense signals relative to the weaker signal has improved the assignment of the weaker multiplet peaks in DQF *J*-RES spectrum.

Regular $^{1}$H NMR with presaturation, regular *J*-RES projection, and DQF *J*-RES projection are compared for the same intensity of the most intense singlet peak in Fig. 3a, b, and c respectively from the AA's mixture. This comparison shows a few intense singlet signals marked with a star (at 3.24, 3.0, 2.26, ppm) dominate the regular $^{1}$H NMR (a) and regular *J*-RES projection (b). In contrast, DQF *J*-RES projection in c shows great improvement in the intensity of the smaller signals relative to the curtailed singlet signals marked with a star. Further, we made a comparison of the regular *J*-RES projection and DQF *J*-RES projection on the same noise level in (d) and (e) respectively which shows much higher signal to noise ratio (S:N) of the regular *J*-RES projection. Measurement of S:N for four peaks reported in SI Table 1 revealed regular *J*-RES has on average much higher S:N relative to the DQF *J*-RES projection. However, the suppression of the intense singlet peaks improves the visibility of the weak intensity metabolite peaks as the receiver gain gets optimized for the smaller signals in DQF *J*-RES spectrum. This is clearer from the analysis of the 2D spectral portions in Fig. 2c-f.

Identification of metabolites from bio-fluids is routinely performed in metabolomics which often aims for identifying potential biomarkers for diseases. However, severe spectral overlap in the $^{1}$H NMR spectra from bio-fluid samples hampers the identification of many metabolite signals. 2D NMR such as *J*-RES, TOCSY, HSQC are suitable for reducing spectral overlap. Despite the higher resolution of 2D NMR, it does not get rid of the overlap issue completely in particular for complex mixtures where hundreds of metabolites are present in widely varying concentrations. Thus our improved DQF *J*-RES technique was further evaluated on human urine and plant extract samples.

### *4.2. Application to a dried fruit extract sample*

A methanol extract of G. Pedunculata dried fruit was targeted with DQF *J*-RES sequence, and the resulting spectrum was compared with the regular *J*-RES spectrum in Fig. 4. Fig. 4(a), (c), (e), and (g) are small portions expanded from regular *J*-RES spectrum. The corresponding regions from the DQF *J*-RES spectrum are shown in Fig. 4(b), (d), (f), and (h) respectively. Full spectra are displayed in SI Fig. S4 A and S4B. Comparison of dotted boxes a vs. a′ and b vs.

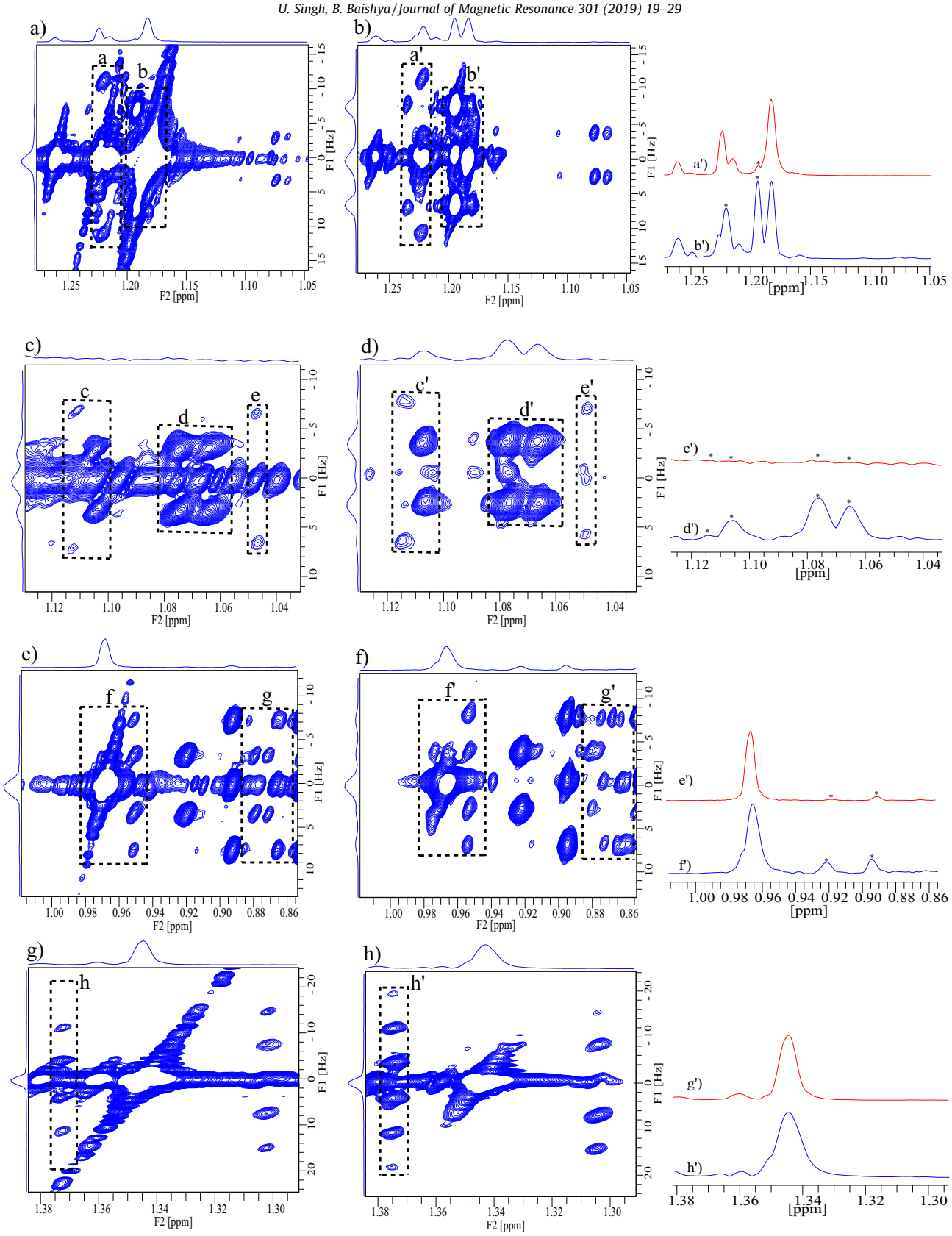


**Fig. 4.** (a), (c), (e), and (g) are small portions expanded from regular *J*-RES spectrum of G. Pedunculata dried fruit extract in methanol. The corresponding regions from the DQF *J*-RES spectrum are shown in Fig. 4(b), (d), (f), and (h) respectively. The intense singlet peaks and its tails along $F_1 = 0$ in regular *J*-RES spectrum are greatly reduced in DQF *J*-RES spectral portions in all panels. Comparison of dotted boxes inside the 2D spectral portions (a) and (b), and their projections on right panels (a′) vs. (b′) shows improved intensity of the multiplets marked with a star in the DQF projection relative to the singlet (shown without star). In (b′) the small hump at the left side of the left star marked peak is actually a reduced singlet peak. The strong singlets in 2D portion (a) have much lower intensity in (b). Similarly comparison of the 2D portions (c) and (d) and their projections (c′) vs. (d′) reveals improved intensity of the multiplets marked with a star in the DQF projection (d′). The absence of the singlets along $F_1 = 0$ is noteworthy in 2D portion (d) relative to (c). Similarly, comparison of (e) vs. (f) and also their projections (e′) vs. (f′) on right panel confirms improved intensity of the multiplets relative to the singlets (marked with a star) and reduced intensity of singlets along $F_1 = 0$ in 2D portion (f). Similarly, the singlets in (g) are also reduced in (h).

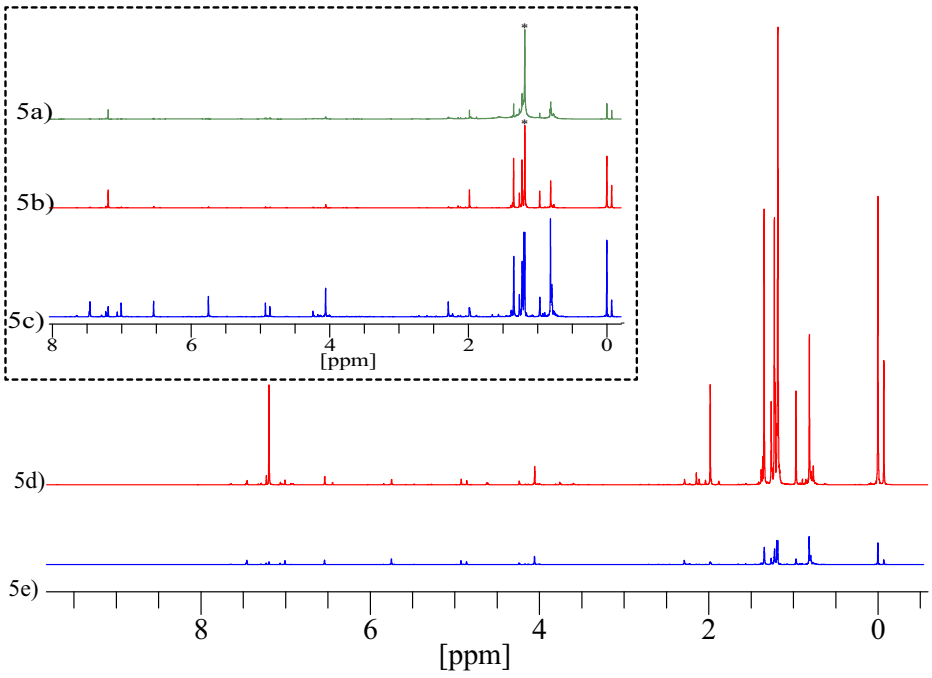


**Fig. 5.** (a)–(c), are the comparison of regular $^1$H NMR with presaturation, regular *J*-RES projection, and DQF *J*-RES projection respectively from the G. Pedunculata dried fruit extract plotted for the same intensity of the most intense singlet peak marked with a star. The intense singlet signals marked with star dominate the spectra in (a) and (b) rendering the smaller signals almost undetectable. In contrast, DQF *J*-RES projection in 5c shows great improvement in the intensity of the smaller signals relative to the intense singlet signals whose intensity is now substantially reduced relative to the other peaks. Comparison on the same noise level of the regular *J*-RES projection and DQF *J*-RES projection is also shown in (5d) and (5e) which indicates much higher S:N of the regular *J*-RES projection. SI table S2 with the S:N values for four peaks indicate regular *J*-RES has much higher S:N relative to the DQF *J*-RES projection although DQF *J*-RES, in this case, was recorded with two times more number of transients. However, the suppression of the intense singlet peaks improves the visibility of the weak intensity metabolite peaks as the maximum receiver gain gets optimised for these smaller signals in DQF *J*-RES spectrum (203 relative to 10 in regular *J*-RES spectrum).

b′ from (4a) and (4b) display better visibility of the multiplets in DQF *J*-RES spectrum in (4b) which are otherwise obscured due to the presence of strong singlet peaks and their intense tails along $F_1 = 0$ in (4a). Two triplets and one doublet are clearly observed inside dotted box a′ and b′ in (4b).

Comparison of Fig. 4(c) and (d) (dotted boxes c vs. c′, d vs. d′, e vs. e′) reveals that regular *J*-RES spectrum is dominated by the intense singlet peaks along $F_1 = 0$ leading to concealing of the multiplet structures from the low abundant metabolites. However, these intense singlet peaks along $F_1 = 0$ get completely suppressed in DQF *J*-RES spectrum in 4d) improving the visibility of the multiplets. Similarly, comparison of the Fig. 4(e) vs. (f), and (g) vs. (h) reveals efficient suppression of the intense singlet peaks along $F_1 = 0$ in the DQF *J*-RES spectrum improving the clarity of the neighboring multiplet peaks. Comparison of the 1D projections from the compared 2D portions (In left and middle panels) are shown on right panels as (a′) vs. (b′), (c′) vs. (d′), (e′) vs. (f′), g′) vs. (h′) respectively (plotted for the comparable intensity of the larger signals)- which further confirms improved visibility of the multiplet peaks marked with star in the DQF projections relative to the singlet peaks (without star) in the regular *J*-RES projections. For instance, the star marked triplets in the projection b′) have poor visibility in the projection a′).

When compared for the same intensity of the most intense singlet peak Fig. 5(a) (regular $^1$H NMR with presaturation), (b) (regular *J*-RES projection), and (c) (DQF *J*-RES projection) reveals that DQF *J*-RES projection in (c) shows great improvement in the intensity of the smaller signals present in the region from 2 to 8 ppm relative to the intense singlet peaks in the region from 0 to 2 ppm. In fact the $^1$H 1D spectrum in Fig. 5(a) is dominated by the singlet marked with a star. Most of these signals (2 to 8 ppm) appear with very poor intensity in regular *J*-RES projection in (b) and in $^1$H 1D in (a) when compared to the intense singlets in the region from 0 to 2 ppm. Due to the suppression of the intense singlet signals, the receiver gain improved in the DQF *J*-RES spectrum which improved the visibility of the low abundant metabolite peaks which were on the noise level in the regular *J*-RES spectrum. Further, a comparison on the same noise level of the regular *J*-RES projection and DQF *J*-RES projection in (d) and (e) shows much higher S:N of the regular *J*-RES projection. The S:N values for four peaks are reported in SI Table 2 which implies regular *J*-RES has on average much higher S:N relative to the DQF *J*-RES projection. However, the suppression of the intense singlet peaks improves the visibility of the weak intensity metabolite peaks as the receiver gain gets optimised for the smaller signals in DQF *J*-RES spectrum to 203 (relative to 10 in regular *J*-RES spectrum). This is clearer from the analysis of the 2D spectral portions in Fig. 4a-f.

### *4.3. Application to a lyophilized human urine sample.*

The performance of the DQF *J*-RES experiment was further evaluated on a lyophilized human urine sample in $D_2O$. While full spectra are reported in the SI Fig. S3A and S3B, representative 2D *J*-RES spectral sections are shown expanded in Fig. 6(a), (c), (e), (g), (i), and (k) from the regular *J*-RES sequence and in (6b), (6d), (6f), (6h), (6j), and (6l) from the DQF *J*-RES sequence.

In Fig. 6a), close to the right side of the dotted line b an intense singlet is present which does not allow any weak intensity multiplets in its vicinity to be noticeable. For example, there are multiplets along the dotted line b and c but are not detectable due to the intense singlet in the middle of these two lines. Suppression of this intense singlet in (6b) allows the multiplets b′, c′, and d′ to be better resolved and their multiplet pattern gets established. While the doublet f is very weak in (6a), its intensity improves in (6b).

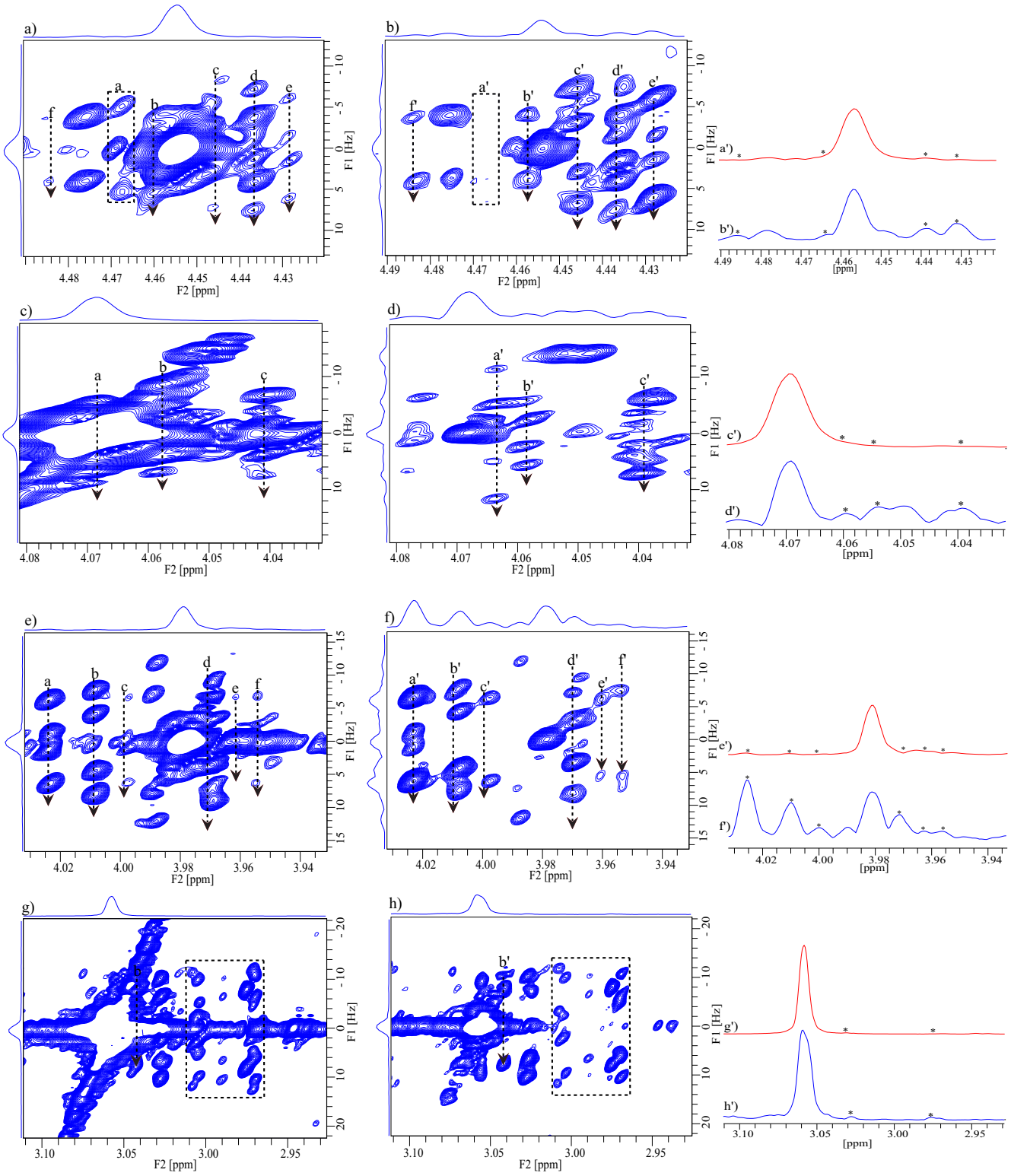


**Fig. 6.** (a), (c), (e), (g), (i), and (k) are small portions expanded from regular *J*-RES spectrum of a lyophilized human urine sample in $D_2O$. The corresponding regions from the DQF *J*-RES spectrum are shown in (b), (d), (f), (h), (j), and (l) respectively. In all spectral portions from regular *J*-RES spectrum (all left side panels), the intense singlets dominate along $F_1 = 0$ which prevents unambiguous determination of a multiplicity of the signals which are overlapped with the singlets. In contrast the corresponding spectral portions from DQF *J*-RES spectrum (all middle panels) uncovers many hidden multiplets such as b′, c′ in (6b) vs. b, c in (6a); a′, b′ in (6d) vs. a, b in (6c); d′ in (6f) vs. d in (6e); b′ in (6h) vs. b in (6g). In addition, many other peaks have greater clarity in the DQF *J*-RES spectrum as detailed in results and discussions. The right panel (topmost) show the comparison between the projections (a′) vs. (b′) extracted from the 2D spectral portions on left (a) and (b) respectively. The enhanced intensity of the multiplets in the DQF projection (b′) are marked with star relative to the singlet shown without a star. These comparisons are for the same intensity of the singlets between (a′) and (b′). Similar results are obtained from the comparison of the other *J*-RES projection (top in each panel) vs. DQF *J*-RES projection (bottom in each panel) viz. (c′) vs. (d′); (e′) vs. (f′); (g′) vs. (h′); (i′) vs. (j′); (k′) vs. (l′).

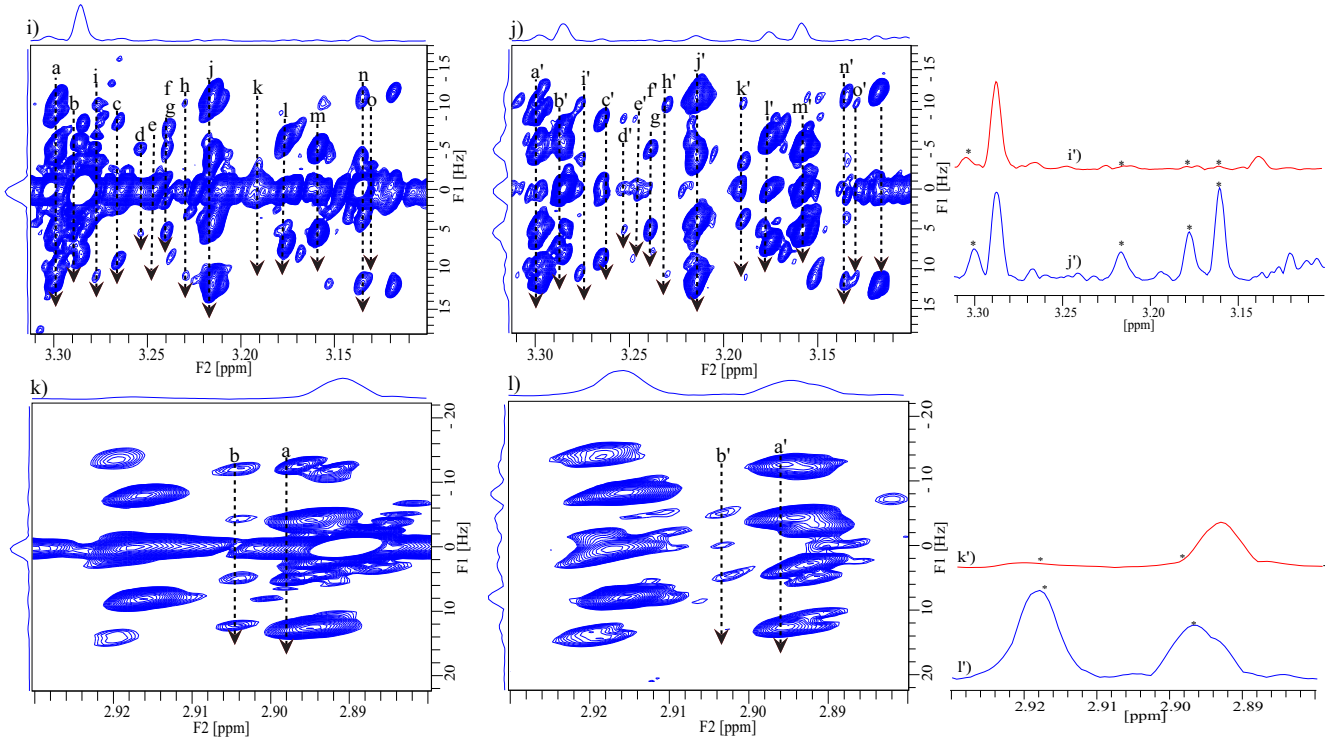


**Fig. 6** (*continued*)

Similarly, the doublet of doublet e′ displays more intensity in 6b) relative to e in (6a). However, doublet a in (6a) is missing in (6b) indicated by the empty dotted box a′. Similarly, the intense singlet from creatinine overlapping the line a in (6c) is almost completely suppressed in (6d). As a result, the two doublet of doublets marked with a′ and b′ are clearly observed in (6d) whereas in (6c) these peaks get completely obscured and lost inside the intense peak. The appearance of the multiplet c′ is also improved in (6d). Similarly, the multiplets a′ to f′ are more clearly detected and established in (6f) relative to the peaks a to f in (6e) due to the suppression of the intense singlets along $F_1 = 0$ by the DQ filter in (6f). Comparison of (6g) and (6h) reveals that the multiplets within the dotted box are more clearly established in (6h) due to the absence of the singlet peaks along $F_1 = 0$. Besides, the multiplet peak b′ is much better visible in (6h) whereas it is almost buried inside the tail of the singlet from creatinine in (6g).

Comparison of the multiplets marked with letters a-o in Fig. 6i) with the corresponding peaks in (6j) marked with letters a′-o′ reveal that the DQF filter effectively suppresses most of the high-intensity singlet signals along $F_1 = 0$ in (6j) and improves the clarity of the multiplets compared to (6i). Multiplet patterns of a′, b′, i′, g′, h′, j′, n′, o′ in (6j) becomes more clear compared to a, b, i, g, h, j, n, o in 6I due to the suppression of the strong singlet signals along $F_1 = 0$. For instance, that c′ is a doublet of doublet and h′ is a doublet becomes unambiguous in (6j) but singlet intensity along $F_1 = 0$ does not allow this to be confirmed in (6i). While doublet d and f are present in (6i), corresponding peaks d′ and f′ are missing in (6j). Similarly, while the peaks k′ and o′ are present in (6j), corresponding peaks k and o are missing in (6i). On fewer occasions a few peaks were found missing in the DQF *J*-RES spectrum, for example, the doublet of doublet b in 6 k) is missing in 6 l). This is further displayed for many other peaks in SI Figures S2 and S3 for plant extract and lyophilized urine samples respectively. Comparison of the 1D projections from the compared 2D portions on the left and middle panels are shown on right panels a′) vs. b′), c′) vs. d′), e′) vs. f′), g′) vs. h′), i′) vs. j′), k′) vs. l′) respectively- which further confirms improved visibility of the multiplet peaks relative to the intense singlet peaks.

In order to address the disappearance of certain multiplet peaks in DQF *J*-RES spectrum, we investigated the delay-dependent modulation of the signals by the DQF. A series of DQF spectra were recorded for different values of delay Δ (20, 30, 40, and 50 ms) on the same lyophilized human urine sample and reported in SI Figure S1. Since, in a metabolomics complex mixture, large variations exist in *J*-values due to the presence of a large number of metabolites; thus some signals can disappear in the DQF *J*-RES spectrum when their sine modulated antiphase precursor terms after a 2Δ period approach zero values. Therefore, for certain *J*-values the creation of double quantum coherence is maximum; however, for other *J*-values, this could be minimum. This situation changes as a function of the delay Δ. As we show in Figure S1 in SI, more multiplets can be recovered by a combined analysis of these DQF *J*-RES spectra recorded with different values of Δ and comparing with each other as well as to the regular *J*-RES. This process is although time-consuming can be more fruitful.

Comparison of the Fig. 7a) (regular $^1$H NMR with presaturation), (7b) (regular *J*-RES projection), and (7c) (DQF *J*-RES projection) reveals that even for the same receiver gain and same acquisition parameters (recycle delay, number of transients were also same in this case, and acquisition time) the DQF *J*-RES projection shows much better visibility of the smaller signals. The intense singlet signals marked with a star at 3.05 ppm and 4.07 ppm (from creatinine) in (7a) and (7b) dominate the $^1$H 1D and regular *J*-RES projection respectively. As a result, very few signals in $^1$H 1D in (7a) and regular *J*-RES projection in (7b) display intensity comparable to the singlet from creatinine. With the suppression of the singlets in (7c), visibility of the weak intensity metabolite peaks are improved. Further, a comparison on the same noise level of the regular *J*-RES projection and DQF *J*-RES projection in (7d) and (7e) shows much higher S:N of the regular *J*-RES projection. The S:N values for five peaks are reported in SI Table 3 which implies regular *J*-RES has on average six to eight times higher S:N relative

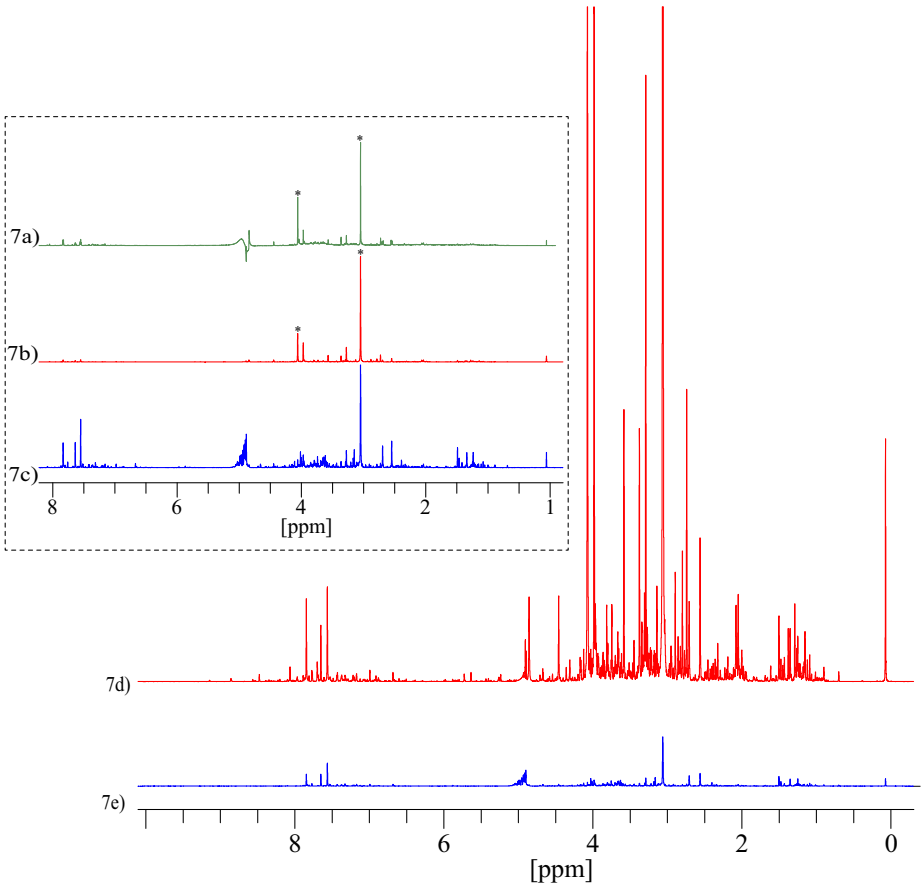


**Fig. 7.** (a)–(c), is a comparison of regular $^{1}$H NMR with presaturation, regular *J*-RES projection, and DQF *J*-RES projection respectively from the lyophilized human urine sample in $D_2O$ displayed for the same intensity of the most intense singlet peak marked with a star. The intense singlet signals marked with star dominate the spectra in (a) and (b) rendering the smaller signals almost undetectable. In contrast, DQF *J*-RES projection in (7c) shows great improvement in the intensity of the smaller signals relative to the intense singlet signals whose intensity is now considerably reduced. Comparison on the same noise level of the regular *J*-RES projection and DQF *J*-RES projection is also shown in (d) and (e) which indicates much higher S:N of the regular *J*-RES projection. SI table S3 with the S:N values for five peaks indicates regular *J*-RES has on average six to eight times higher S:N relative to the DQF *J*-RES projection (DQF *J*-RES, in this case, was recorded with the same number of transients as regular *J*-RES). However, the suppression of the intense singlet peaks improves the visibility of the weak intensity metabolite peaks as the dynamic range limitation is much less in the DQF *J*-RES spectrum.

to the DQF *J*-RES projection. However, the suppression of the intense singlet peaks improves the visibility of the weak intensity metabolite peaks as the receiver gain gets optimised for the smaller signals in DQF *J*-RES spectrum.

## 5. Conclusion

We have demonstrated a novel pulse technique – the DQF *J*-RES spectroscopy which overcomes the limitations of regular *J*-RES experiments when applied to complex mixtures, where large singlet components of a few signals obscure neighboring important multiplet peaks and also lowers their intensity due to the dynamic range issues. The new technique could clearly identify many important multiplet peaks from sparsely present metabolites in various complex mixtures such as urine and plant extract samples. The new method not only suppressed the intense singlet peaks but also improved the visibility of the weaker multiplet peaks as the receiver gain could be raised in the absence of the strong singlet signals such as creatinine and other peaks in urine. When compared for the same noise level, the DQF *J*-RES, in general, displayed six to eight fold reduced S:N, however, the signals are much larger than the noise due to reduced digitization noise. This combined with the significantly reduced intensity of the strong singlet peaks improve the spectral readout of the weaker multiplets in DQF *J*-RES spectra. While most of the signals in each complex mixture studied were better resolved in the DQF *J*-RES spectrum; however, a few peaks were absent, which could be detected in regular *J*-RES spectrum. This effect was also systematically studied for various values of the DQF period and revealed more information on the multiplets could be acquired by recording a series of DQF *J*-RES spectra with a few different delays for the DQ filter period. Thus a combined analysis using regular *J*-RES and DQF *J*-RES with different delays may be more fruitful.

## Acknowledgments

Upendra Singh thanks UGC (University Grants Commission) India, for a research fellowship. We thank the Science and Engineering Research Board (SERB) under the Department of Science & Technology (DST), Govt. Of India, DST No: EMR/2014/001280 (Grant No. SERB/F/6435/2015-16) for the extramural research grant.

## Appendix A. Supplementary material

Supplementary data to this article can be found online at https://doi.org/10.1016/j.jmr.2019.02.003.

## References


[1] J.M. Fonville, A.D. Maher, M. Coen, E. Holmes, J.C. Lindon, J.K. Nicholson, Evaluation of full-resolution J-resolved 1H NMR projections of biofluids for metabonomics information retrieval and biomarker identification, Anal. Chem. 82 (2010) 1811–1821.

[2] P.J.D. Foxall, J.A. Parkinson, I.H. Sadler, J.C. Lindon, J.K. Nicholson, Analysis of biological fluids using 600 MHz proton NMR spectroscopy: application of homonuclear two-dimensional J-resolved spectroscopy to urine and blood plasma for spectral simplification and assignment, J. Pharm. Biomed. Anal. 11 (1993) 21–31.

[3] P.J.D. Foxall, M. Spraul, R.D. Farrant, L.C. Lindon, G.H. Neild, J.K. Nicholson, 750 MHz $^{1}$H-NMR spectroscopy of human blood plasma, J. Pharm. Biomed. Anal. 11 (1993) 267–276.

[4] B.C. Sweatman, R.D. Farrant, E. Holmes, F.Y. Ghauri, J.K. Nicholson, J.C. Lindon, 600 MHz 1H-NMR spectroscopy of human cerebrospinal fluid: Effects of sample manipulation and assignment of resonances, J. Pharm. Biomed. Anal. 11 (1993) 651–664.

[5] M.J. Lynch, J. Masters, J.P. Pryor, J.C. Lindon, M. Spraul, P.J.D. Foxall, J.K. Nicholson, Ultra high field NMR spectroscopic studies on human seminal fluid, seminal vesicle and prostatic secretions, J. Pharm. Biomed. Anal. 12 (1994) 5–19.

[6] H. Antti, T.M.D. Ebbels, H.C. Keun, M.E. Bollard, O. Beckonert, J.C. Lindon, J.K. Nicholson, E. Holmes, Statistical experimental design and partial least squares regression analysis of biofluid metabonomic NMR and clinical chemistry data for screening of adverse drug effects Chemom, Intell. Lab. Syst. 73 (2004) 139–149.

[7] M.R. Viant, C. Ludwig, S. Rhodes, U.L. Guenther, D. Allaway, Validation of a urine metabolome fingerprint in dog for phenotypic classification, Metabolomics 3 (2007) 453–463.

[8] M.R. Viant, Improved methods for the acquisition and interpretation of NMR metabolomic dat, Biochem. Biophys. Res. Commun. 310 (2003) 943–948.

[9] J.K. Nicholson, P.J.D. Foxall, M. Spraul, R.D. Farrant, J.C. Lindon, 750 MHz 1H and 1H–13C NMR spectroscopy of human blood plasma, Anal. Chem. 67 (1995) 793–811.

[10] H.T. Widarto, E. Van der Meijden, A.W.M. Lefeber, C. Erkelens, K. Kim, H.Y.H. Choi, R. Verpoorte, Metabolomic differentiation of Brassica rapa following herbivory by different insect instars using two-dimensional nuclear magnetic resonance spectroscopy, J. Chem. Ecol. 32 (2006) 2417–2428.

[11] M.R. Viant, J.G. Bundy, C.A. Pincetich, J.S. de Ropp, R.S. Tjeerdema, NMR-derived developmental metabolic trajectories: an approach forvisualizing the toxic actions of trichloroethylene during embryogenesis, Metabolomics 1 (2005) 149–158.

[12] A. Khatib, E.G. Wilson, H.K. Kim, A.W.M. Lefeber, C. Erkelens, Y.H. Choi, R. Verpoorte, Application of two-dimensional J-resolved nuclear magnetic resonance spectroscopy to differentiation of beer, Anal. Chim. Acta 559 (2006) 264–270.

[13] C.H. Johnson, T.J. Athersuch, I.D. Wilson, L. Iddon, X.L. Meng, A.V. Stachulski, J. C. Lindon, J.K. Nicholson, kinetic and J-resolved statistical total correlation NMR spectroscopy approaches to structural information recovery in complex reacting mixtures: application to acyl glucuronide intramolecular transacylation reactions, Anal. Chem. 80 (2008) 4886–4895.

[14] Y.L. Wang, M.E. Bollard, H. Keun, H. Antti, O. Beckonert, T.M. Ebbels, J.C. Lindon, E. Holmes, H.R. Tang, J.K. Nicholson, Spectral editing and pattern recognition methods applied to high-resolution magic-angle spinning $^{1}$H nuclear magnetic resonance spectroscopy of liver tissues, Anal. Biochem. 323 (2003) 26–32.

[15] J. Farjon, D. Merlet, P. Lesot, J. Courtieu, Enantiomeric excess measurements in weakly oriented chiral liquid crystal solvents through 2D 1H selective refocusing experiments, J. Magn. Reson. 158 (2002) 169–172.

[16] K. Kobzar, H. Kessler, B. Luy, Stretched gelatin gels as chiral alignment media capable to discriminate enantiomers, Angew. Chem. Int. Ed. 44 (2005) 3145–3147. Corrigendum: Angew, Chem. Int. Ed. 44 (2005) 3509.

[17] S.R. Chaudhari, N. Suryaprakash, Chiral discrimination and the measurement of enantiomeric excess from a severely overcrowded NMR spectrum, Chem. Phys. Lett. 555 (2013) 286–290.

[18] B. Luy, J.P. Marino, JE-TROSY: comined J- and TROSY-spectroscopy for the measurement of one-bond couplings in macromolecules, J. Magn. Reson. 163 (2003) 92–98.

[19] J. Furrer, M. John, H. Kessler, B. Luy, J-spectroscopy in the presence of residual dipolar couplings: determination of one-bond coupling constants and separate dimension with scalable resolution, J. Biomol. NMR 37 (2007) 231–243.

[20] M. Nilsson, G.A. Morris, Pure shift proton DOSY: diffusion-ordered 1H spectra without multiplet structure, Chem. Commun. 9 (2007) 933–935.

[21] A.J. Pell, J. Keeler, Two-dimensional J-spectra with absorption-mode lineshapes, J. Magn. Reson. 189 (2007) 293–299.

[22] S. Simova, H. Sengstschmid, R. Freeman, Proton chemical-shift spectra, J. Magn. Reson. 124 (1997) 104–121.

[23] A. Bax, A.F. Mehlkopf, J. Smidt, A fast method for obtaining 2D J-resolved absorption spectra, J. Magn. Reson. 40 (1980) 213–219.

[24] V.A. Mandelshtam, Q.N. Van, A.J. Shaka, Obtaining proton chemical shifts and multiplets from several 1D NMR signals, J. Am. Chem. Soc. 120 (1998) 12161–12162.

[25] B. Luy, Adiabatic z-filtered J-spectroscopy for absorptive homonuclear decoupled spectra, J. Magn. Reson. 201 (2009) 18–24.

[26] A. Verma, B. Baishya, Real-time band-selective homonuclear proton decoupling for improving sensitivity and resolution in phase-sensitive J-resolved spectroscopy, ChemPhysChem. 16 (2015) 2687–2691.

[27] M. Foroozandeh, R.W. Adams, P. Kiraly, M. Nilsson, G.A. Morris, Measuring couplings in crowded NMR spectra: pure shift NMR with multiplet analysis, Chem. Commun. (2015) 1–3.

[28] A. Verma, B. Baishya, Real-time bilinear rotation decoupling in absorptive mode J-spectroscopy: detecting low-intensity metabolite peak close to high-intensity metabolite peak with convenience, J. Magn. Reson. 266 (2016) 51–58.

[29] S.H. Smallcombe, S.L. Patt, P.A. Keifer, WET solvent suppression and its applications to LC NMR and high-resolution NMR spectroscopy, J. Magn. Reson. Series A 117 (1995) 295–303.

[30] M. Rance, O.W. Sørensen, G. Bodenhausen, G. Wagner, R.R. Ernst, K. Wüthrich, Improved spectral resolution in COSY 1H NMR spectra of proteins via double quantum filtering, Biochem. Biophys. Res. Commun. 117 (1983) 479–485.

[31] U. Piantini, O.W. Sørensen, R.R. Ernst, Multiple quantum filters for elucidating NMR coupling networks, J. Am. Chem. Soc. 104 (1982) 6800–6801.

[32] A.J. Shaka, R. Freeman, Simplification of NMR spectra by filtration through multiple- quantum coherence, J. Magn. Reson. 51 (1983) 169–173.

[33] N. Müller, R.R. Ernst, K. Wüthrich, Multiple-quantum-filtered two-dimensional correlated NMR spectroscopy of proteins, J. Am. Chem. Soc. 108 (1986) 6482–6492.

[34] P.C.M. van Zijl, M. O'Neil Johnson, S. Mori, R.E. Hurd, Magic-angle-gradient double-quantum-filtered COSY, J. Magn. Reson., Ser A 113 (1995) 265–270.

[35] A.L. Davis, E.D. Laue, J. Keeler, D. Moskau, J.J. Lohman, Absorption-mode two dimensional NMR spectra recorded using pulsed field gradients, J. Magn. Reson. 94 (1991) 637–644.

[36] Jacob M. Newman, Alexej Jerschow, Improvements in complex mixture analysis by NMR: DQF-COSY iDOSY, Anal. Chem. 79 (2007) 2957–2960.

[37] Y. Huang, S. Cai, Z. Zhang, Z. Chen, High-resolution two-dimensional J-resolved NMR spectroscopy for biological systems, Biophys. J. 106 (2014) 2061–2070.

[38] Y. Huang, Z. Zhang, H. Chen, J. Feng, S. Cai, Z. Chen, A high-resolution 2D J-resolved NMR detection technique for metabolite analyses of biological samples, Sci. Reports 5 (2015) 8390.